NF-κB dysregulation in microRNA-146a–deficient mice drives the development of myeloid malignancies

Jimmy L. Zhao[a,1], Dinesh S. Rao[a,b,1], Mark P. Boldin[c], Konstantin D. Taganov[d], Ryan M. O'Connell[a], and David Baltimore[a,2]

[a]Division of Biology, California Institute of Technology, Pasadena, CA 91125; [b]Department of Pathology and Laboratory Medicine, The David Geffen School of Medicine, University of California, Los Angeles, CA 90095; [c]Department of Molecular and Cellular Biology, Beckman Research Institute, City of Hope, Duarte, CA 91010; and [d]Regulus Therapeutics Inc., San Diego, CA 92121

MicroRNA miR-146a has been implicated as a negative feedback regulator of NF-κB activation. Knockout of the *miR-146a* gene in C57BL/6 mice leads to histologically and immunophenotypically defined myeloid sarcomas and some lymphomas. The sarcomas are transplantable to immunologically compromised hosts, showing that they are true malignancies. The animals also exhibit chronic myeloproliferation in their bone marrow. Spleen and marrow cells show increased transcription of NF-κB–regulated genes and tumors have higher nuclear p65. Genetic ablation of NF-κB p50 suppresses the myeloproliferation, showing that dysregulation of NF-κB is responsible for the myeloproliferative disease.

inflammation | cancer | myelofibrosis | noncoding RNA

MicroRNAs are a group of ~19- to 23-nucleotide long non-coding RNAs that repress target gene expression by a combination of mRNA degradation and translation inhibition (1). Recent studies have revealed important physiological roles of miRNAs in many aspects of mammalian hematopoiesis and immune cell function, and their altered expression has been linked to pathological conditions of the immune system, such as hematologic cancers and autoimmunity (2–4).

Chronic inflammation contributes to cancer initiation and progression. Among a myriad of proposed mechanisms linking inflammation to cancer, NF-κB has been identified as a key mediator of inflammation-induced carcinogenesis (5). Moreover, constitutive NF-κB activation is frequently detected in many types of lymphoid and myeloid malignancies (6, 7). Hence, understanding how NF-κB activity is down-regulated has been a focus of study with important advances in recent years (8). In particular, NF-κB regulation by noncoding RNAs has recently begun to be characterized. A few years ago, we carried out a microarray screen to identify miRNAs induced by NF-κB activation and miR-146a was discovered to be one of the miRNAs induced by LPS in a human monocytic cell line. The induction of miR-146a was shown to be NF-κB–dependent, and upon induction, miR-146a functioned to directly down-regulate TNF receptor-associated factor 6 (TRAF6) and IL-1 receptor-associated kinase 1 (IRAK1), two of the signal transducers in the NF-κB activation pathway (9). Based on this study and others (10, 11), we hypothesized that miR-146a, by repressing TRAF6 and IRAK1, may have an effect on NF-κB activation, dampening or terminating an inflammatory response via a negative-feedback loop. To definitively characterize the function of miR-146a in vivo and directly test the hypothesis that miR-146a is a negative regulator of the NF-κB pathway, we generated two independent mouse strains with a targeted germ-line deletion of miR-146a, one on the mixed C57BL/6 × 129/sv background and one on the pure C57BL/6 background. Initial study done primarily with the mixed background miR-146a$^{-/-}$ mice showed that miR-146a$^{-/-}$ mice were hypersensitive to LPS challenge, and aging miR-146a$^{-/-}$ mice developed autoimmune-like disease, myeloid proliferation in their spleens, and hematopoietic tumors (12). However, the cellular lineage of the tumors and the mechanistic basis of miR-146a–deficiency mediated myeloproliferation remained important unanswered questions. In addition, the relationship of the

tumor phenotype in miR-146a$^{-/-}$ mice and NF-κB dysregulation was uncertain because of the multiple potential targets of miR-146a in different molecular pathways. Here, we focus on characterizing the incidence, cellular lineage, and transplantability of the tumors, and to understand the molecular basis of oncogenesis.

We have found that when they are allowed to age naturally, miR-146a$^{-/-}$ mice on a pure C57BL/6 background develop a chronic inflammatory phenotype with progressive myeloproliferation involving both the spleen and the bone marrow, which eventually progresses to splenic myeloid sarcoma and bone marrow failure at about 18 mo of age. Lymphomas of either a B-cell lineage or a mixed T- and B-cell lineage are also observed in older miR-146a$^{-/-}$ mice at a much higher frequency than in wild-type animals. Myeloproliferation in miR-146a–deficient mice are driven primarily by the action of NF-κB because reduction in the NF-κB level by deletion of the NF-κB subunit p50 effectively suppresses the pathology. Thus, we have provided genetic evidence that miR-146a functions as a tumor suppressor in both myeloid and lymphoid cells and that chronic NF-κB activation as a result of miR-146a–deficiency is responsible for driving the myeloproliferative disease, which can progress to malignant myeloid sarcoma.

Results

miR-146a Knockout Mice Develop Myeloid and Lymphoid Malignancies. The miR-146a–deficient pure C57BL/6 mouse was made by deleting about 300 base pairs of genomic DNA fragment containing the miR-146a precursor (12). The miR-146a–deficient mice (homozygous knockouts, designated as miR-146a KO) were born at the expected Mendelian frequency and appeared to be normal at birth. However, starting at about 5 to 6 mo of age, they developed progressively enlarged spleens. By 18 to 22 mo of age, 80% of the KO mice were moribund and were culled for analysis. However, the entire cohort of age-matched littermate C57BL/6 (WT) control mice, except for one case of thymoma and one case of seizure, were still alive and healthy (Fig. S1A). On necropsy, KO mice demonstrated various degrees of splenomegaly, with KO spleens on average weighing six to seven times more than wild-type spleens (Fig. S1 B and C). By FACS analysis, splenomegaly was correlated with a massive expansion of the CD11b$^+$ myeloid population (Fig. S1 D–F). Expanded splenic hematopoiesis was also noted based on the increased Ter119$^+$ erythroid precursor population in the spleen. About 40% of the mice demonstrated distinct splenic tumors (Fig. 1 A and B). The majority of these tumors displayed the histologic appearance of a myeloid sarcoma

---

Fig. 1. miR-146a–deficient mice develop myeloid and lymphoid malignancies. Mice were 18- to 22-mo-old miR-146a$^{-/-}$ mice (KO) and sex- and age-matched C57BL/6 control mice (WT). (A) Incidences of myeloid and lymphoid malignancies observed in wild-type (n = 39) and KO (n = 43) mice. (B) Photograph, FACS plot, and histological analysis of a representative myeloid tumor from a KO spleen. Panels 3 and 4 show an H&E-stained spleen section. [Scale bars, (Left) 100 μm; (Right) 40 μm.] Arrows, mitotic figures. (C) Photograph, FACS plot, and histological analysis of a representative B-cell lymphoma from a KO gastrointestinal tract. Panels 3 and 5 show an H&E-stained tumor section; panel 4 shows positive immunohistochemical staining for B220 [Scale bars, (Left to Right) 100 μm in panels 3 and 4 and 40 μm in panel 5.] (D) Photograph, FACS plot, and histological analysis of a representative mixed T- and B-cell lymphoma from a KO liver. Panels 3–5 show H&E-stained liver sections. Lym, Lymphoma; Liv, relatively uninvolved liver. [Scale bars (Left to Right) are 400 μm, 100 μm, and 40 μm.]

IMMUNOLOGY

(Fig. 1B) (13). FACS analysis of carefully dissected tumors showed that the cells derived from these tumors expressed the pan-myeloid antigen, CD11b (Fig. 1B). Occasionally, liver and kidney were also heavily infiltrated by myeloid sarcoma (Fig. S2 A and B). A general role of miR-146a as a tumor-suppressor miRNA in the hematolymphoid system was demonstrated by the development of lymphomas of a B-cell or a mixed T- and B-cell lineage in the cervical lymph node, gastrointestinal tract, liver, and kidney in about 20% of the KO mice (Fig. 1A). Similar lymphoid tumors were not identified in wild-type mice. The lineage of these tumors was confirmed by FACS as well as immunohistochemical stains (Fig. 1 C and D and Fig. S2 C and D). Histological analysis revealed that the lymphomas ranged from low-grade follicular lymphoma (Fig. S2C) to high-grade diffuse large B-cell lymphoma with apoptotic bodies and atypical mitosis (Fig. 1C and Fig. S2D).

Myeloid Tumors Are Transplantable into Immunocompromised Recipient Mice. The ability of a mass of cells to form tumors upon transplantation to a secondary mouse can distinguish a malignant growth from a reactive inflammatory process. KO splenic tumor cells dissected from the tumor nodules in the spleen and wild-type control spleen cells were transplanted into immunocompromised Rag2$^{-/-}$γC$^{-/-}$ BALB/c recipient mice intravenously, with or without transduction by a retrovirus expressing enhanced GFP and luciferase protein. For experiments with retroviral transduction, bioluminescent imaging was used as a sensitive method to track luciferase expression by the transplanted cells in vivo in recipient mice. Starting 1 to 2 wk after intravenous injection, KO splenocytes showed markedly increased proliferation compared with wild-type splenocytes in recipient mice (Fig. 2A). When whole-body bioluminiscence intensity was quantified over

the course of 8 wk, mice receiving KO splenocytes showed a progressive increase in signal, culminating in an ~10- to 20-fold higher signal, indicating a proliferation of the transplanted cells, but wild-type cells did not (Fig. 2B). Interestingly, recipient spleens, kidneys, and livers showed the strongest bioluminiscence signal, indicating the proclivity of transplanted splenic tumor cells to localize to the same organs where the most significant myeloid tumor pathology was observed in the original KO mice. By 2 mo following transplantation, most KO recipient mice became cachectic and moribund, and wild-type recipient mice showed some mild weight loss. In mice receiving KO spleen cells, but not in those receiving wild-type spleen cells, necropsy revealed significant myeloid pathologies, including enlarged spleens and massive infiltration of kidneys and livers by neoplastic myeloid cells (Fig. 2 C–E). Interestingly, not every KO spleen was transplantable. Transplantation of age-matched KO splenocytes from mice without overt myeloid sarcoma did not result in significant myeloid pathology in recipient mice, suggesting there is a qualitative difference (e.g., additional mutations) between KO spleens with myeloproliferation and those with overt myeloid sarcoma.

Chronic Myeloproliferation and Myelofibrosis in miR-146a–Deficient Bone Marrow. In addition to splenic myeloproliferation and myeloid sarcoma, the bone marrow of miR-146a KO mice showed significant myeloproliferative disease. By 18 to 22 mo of age, the CD11b^{+} population accounted for 80% of all nucleated bone marrow cells, and the percentages of CD19^{+} B cells dropped to below 10% in miR-146a KO mice (Fig. 3 A and B). In line with the myeloid-dominated bone marrow, peripheral blood showed significant lymphopenia, anemia, and thrombocytopenia, but preserved granulocyte numbers (Fig. 3C and Fig. S3A).

Fig. 2. Myeloid sarcoma is transplantable into immunocompromised Rag2$^{-/-}$γC$^{-/-}$ recipient mice, causing lethal myeloid pathology. WT designates Rag2$^{-/-}$γC$^{-/-}$ mice transplanted with wild-type splenocytes; KO designates Rag2$^{-/-}$γC$^{-/-}$ mice transplanted with miR-146a KO splenocytes ($n = 4$ for wild-type and $n = 4$ for KO; data are representative of three independent experiments). (*A*) Representative bioluminescence images of Rag2$^{-/-}$γC$^{-/-}$ recipient mice splenic side view. (*B*) Quantification of whole-body bioluminescence intensity from splenic side view of one representative experiment. Vertical axis is in logarithmic scale. Transduction efficiency is determined by flow cytometric analysis of GFP$^+$ cells before injection. The bioluminescence intensity is normalized to the percentage of initially transduced cells. (*C*) Spleen weight of Rag2$^{-/-}$γC$^{-/-}$ recipient mice (Student *t* test, *$P < 0.05$). (*D*) Photographs of spleens, kidneys, and livers from representative Rag2$^{-/-}$γC$^{-/-}$ recipient mice. (*E*) Flow cytometric analysis of myeloid cells (defined as CD11b$^+$) in representative recipient kidneys and livers. SSC, side scatter.

In addition, the expanded CD11b$^+$ population in both bone marrow and spleen was also predominantly Gr1$^+$. An increased expression of macrophage colony stimulating factor receptor (CSF1R) was also noted in the myeloid population in both spleen and peripheral blood (Fig. S3*B*). By 18 to 22 mo of age, wild-type bone marrow showed partial replacement of bone marrow cells by adipose tissue as a result of aging, but KO bone marrow showed end-stage fibrosis or a hypercellular bone marrow. The end-stage KO bone marrow was markedly pale by gross analysis, and histologic sections demonstrated paucicellular marrow with thickened bone and fibrosis (Fig. 3*D* and Fig. S3*C*). This chronic myeloproliferation resembles in some ways human myeloproliferative diseases that result in an end stage of marrow fibrosis.

Spleen and Bone Marrow Cells from miR-146a–Deficient Mice Show Increased Activation of NF-κB–Mediated Transcription. We and others have previously identified TRAF6 and IRAK1 as targets of miR-146a in various cell types, including monocytes and macrophages (9, 11). Because TRAF6 and IRAK1 are signal transducers upstream of NF-κB activation, their derepression in miR-146a–deficient mice could result in increased activation of NF-κB. In fact, we have recently demonstrated that TRAF6 and IRAK1 are derepressed in miR-146a KO mice (12). Therefore, we investigated whether increased NF-κB activation might be a feature of the myeloproliferation or myeloid sarcoma in the miR-146a–deficient mice. We extracted RNA from total nucleated spleen cells and total nucleated bone marrow cells and examined RNA expression levels for some genes well known to be NF-κB–responsive, including IL-6, TNF-α, monocyte-chemotactic protein 1 (Mcp1), A20, and the NF-κB subunit p50 (Nfkb1). In the absence of ex vivo stimulation, KO splenocytes and bone marrow cells showed basally up-regulated expression of a subset of NF-κB–responsive genes compared with the wild-type control, suggesting the presence of constitutively activated NF-κB (Fig. 4 *A* and *B*). For some of the genes, such as TNF-α and Mcp1, the expression was even higher in tumor cells isolated from the KO spleen (Fig. 4*A*). To exclude the possibility that a different cellular composition is responsible for the difference, especially in spleens where KO spleens showed a threefold increase in CD11b$^+$ myeloid population, we purified the CD11b$^+$ population from wild-type and KO spleens by magnetic bead-

labeled cell separation (MACS). When the enriched CD11b$^+$ splenocyte population was subjected to the same gene-expression analysis, NF-κB–activated genes, including TNF-α and Mcp1, were still up-regulated in the KO population compared with the wild-type control (Fig. 4*C*). To further confirm the status of NF-κB activation, we assessed the level of nuclear translocation of the NF-κB subunit, RelA (p65), by Western blot analysis of the nuclear protein extract from total nucleated splenocytes. KO splenocytes showed a 1.5- to 2-fold higher level of nuclear p65 than wild-type splenocytes, confirming the activated status of NF-κB (Fig. 4*D*). It is important to note that not every KO spleen showed constitutively higher level of nuclear p65 protein. Increased nuclear p65 correlated well with the presence of myeloid sarcoma (Fig. S4), suggesting that the activation of the NF-κB becomes constitutive only when the KO spleen progresses from myeloproliferation to myeloid sarcoma.

Reduction in the NF-κB Level Rescues the Myeloproliferation in Spleen and Bone Marrow. Both gene expression and nuclear protein analysis indicated that the KO spleen and bone marrow cells showed increased NF-κB activation. To investigate whether activated NF-κB is a causal factor in the observed myeloproliferation, we bred the miR-146a KO strain with an Nfkb1 (p50) KO strain to generate the double transgenic strain with homozygous deletion in both miR-146a and the p50 subunit. p50$^{-/-}$ mice show no developmental abnormality in the immune system and elsewhere but display defective B-cell proliferation and specific antibody production. Cytokine production, including IL-6, TNF-α, and IL-1α, from LPS-stimulated macrophage is also impaired (14, 15). When we intercrossed double heterozygotes for the two KO genes, the various genotypes were born at the expected Mendelian frequency (Fig. S5*A*) and showed no overt abnormalities. Littermates from different genotype groups, miR-146a$^{+/+}$ p50$^{+/+}$ (WT), miR-146a$^{-/-}$ p50$^{+/+}$ (miRKO), miR-146a$^{-/-}$ p50$^{+/-}$ (miRKO p50HET), and miR-146a$^{-/-}$ p50$^{-/-}$ (DKO), were aged to 6 to 7 mo and then were killed for analysis for the development of myeloproliferation in spleen and bone marrow. As expected, by 6 to 7 mo of age, miR-146a KO mice started to develop splenomegaly and myeloproliferation. Importantly, splenomegaly and myeloproliferative disease were significantly reduced in the miR-146a$^{-/-}$ p50$^{+/-}$ group, with the exception of a few outliers. The rescue from the myeloproliferative phenotype
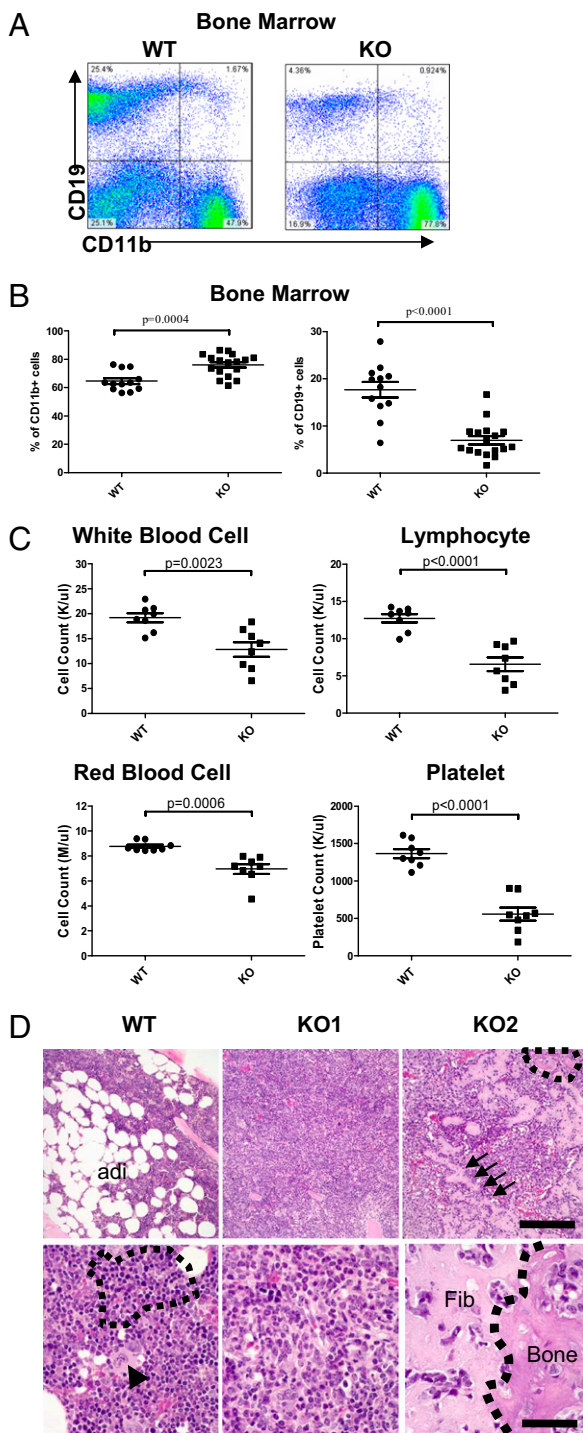
Fig. 3. Chronic myeloproliferation and myelofibrosis occur in miR-146a–deficient bone marrow. Mice were 18- to 22-mo-old miR-146a$^{-/-}$ mice (KO) and sex- and age-matched wild-type control mice (WT). Data are shown as Mean ± SEM. Each individual dot represents one individual mouse. (*A*) Flow cytometric analysis of nucleated bone marrow cells from one representative wild-type mouse and one representative KO mouse for B cells (defined as CD19$^+$) and myeloid cells (defined as CD11b$^+$). (*B*) Percentage of B cells (defined as CD19$^+$) and myeloid cells (defined as CD11b$^+$) in nucleated bone marrow cells by flow cytometric analysis (*n* = 12 for WT and *n* = 17 for KO from at least three independent experiments). (*C*) Absolute numbers of total white blood cells, lymphocytes, red blood cells, and platelets by complete blood count analysis (*n* = 8 for WT and *n* = 8 for KO). (*D*) Representative H&E-stained tibia sections from KO mice showing myelofibrosis and wild-type control. WT, wild-type bone marrow; adi, adipose tissue. KO1, markedly

was more consistent in the miR-146a$^{-/-}$ p50$^{-/-}$ double knockout (DKO) group, as indicated by the reduction in spleen weight and the lack of myeloid cell expansion in the spleen and bone marrow (Fig. 5). In contrast to the pale, fibrotic bone marrow observed in miRKO femurs, the bone marrow in DKO mice was a vibrant red color, similar to what was observed routinely in wild-type mice (Fig. S5*B*). In the spleens of DKO mice, there was also significant reduction in Ter119$^+$ cells relative to miRKO mice, suggesting that expanded splenic hematopoiesis was also rescued by the deletion of p50 in DKO mice (Fig. 5*B*). We conclude that activated NF-κB as a result of miR-146a deletion is the primary factor driving myeloproliferation in miR-146a–deficient mice, because reduction in the NF-κB level by deleting the NF-κB subunit p50 effectively rescues the myeloproliferative phenotype.

Discussion

These results and our previous article (12) demonstrate that miR-146a plays an important role as a tumor suppressor miRNA in hematopoietic lineages because chronic miR-146a–deficiency in mice leads to myeloid sarcomas in spleens and lymphomas in various organs. miR-146a controls myeloproliferation in both the spleen and bone marrow compartments primarily through negatively regulating NF-κB. NF-κB is known to activate many genes involved in inflammation so that this study provides direct evidence correlating the chronic inflammation caused by activated NF-κB and the development of progressive myeloproliferative disease.

Consistent with the initial observation of miR-146a KO mice on the mixed C57BL/6 × 129/sv genetic background (12), miR-146a KO mice on the pure C57BL/6 background developed progressive myeloproliferation in their spleens, although the onset was delayed compared with the mixed background mice. miR-146a KO on the pure C57BL/6 background also developed significant myeloproliferative disease in the bone marrow, which was not observed in the mixed background strain. Moreover, miR-146a KO mice on the pure C57BL/6 background displayed less severe autoimmune-like disease but developed a higher incidence of tumor later in life. All these data indicate that the genetic background can significantly influence the phenotypic manifestation of deleting the miR-146a KO gene.

It is interesting that miR-146a–deficient mice showed no obvious abnormality early on when left unchallenged but gradually developed myeloproliferation in both spleen and bone marrow compartments, starting at about 5 to 6 mo of age. Eventually, more than 50% of the mice developed myeloid sarcomas and lymphomas at about 18 to 22 mo of age. miR-146a normally down-regulates TRAF6 and IRAK1, and in the miR-146a–deficient mice, derepression of these important signal transducers may increase signaling to the NF-κB pathway. It should be noted that overexpression of TRAF6 or IRAK1 in the 293 human embryonic kidney cell line is able to activate NF-κB (16, 17), suggesting a possibility of cell-intrinsic activation of NF-κB when TRAF6 or IRAK1 is overexpressed at a high level. However, this is unlikely to be the case in miR-146a KO mice. We believe that the NF-κB activation in miR-146a KO mice likely involves external stimulation from other cells (autoimmune stimuli) or from environmental pathogens/commensal bacteria for TRAF6/IRAK1 to amplify the signal, and that the mechanism of myeloproliferation and oncogenesis requires repeated episodes of activation of NF-κB from external stimulation. In support of this notion, our previous article reports an increased

hypercellular KO bone marrow that contains virtually no megakaryocytres (arrowhead, *Lower Left*) or erythroid islands (outlined by dashed line, *Lower Left*). KO2: fibrotic KO bone marrow; arrows in the *Upper Right*, a broad band of fibrosis, of which there are many in this field; within the dotted line, an area of new bone formation that may represent end-stage fibrosis; (*Lower Right*) the interface between an area of fibrosis (fib) with entrapped myeloid cells and new bone formation (bone). [Scale bars, (*Upper*) 200 microns; (*Lower*) 40 μm.]
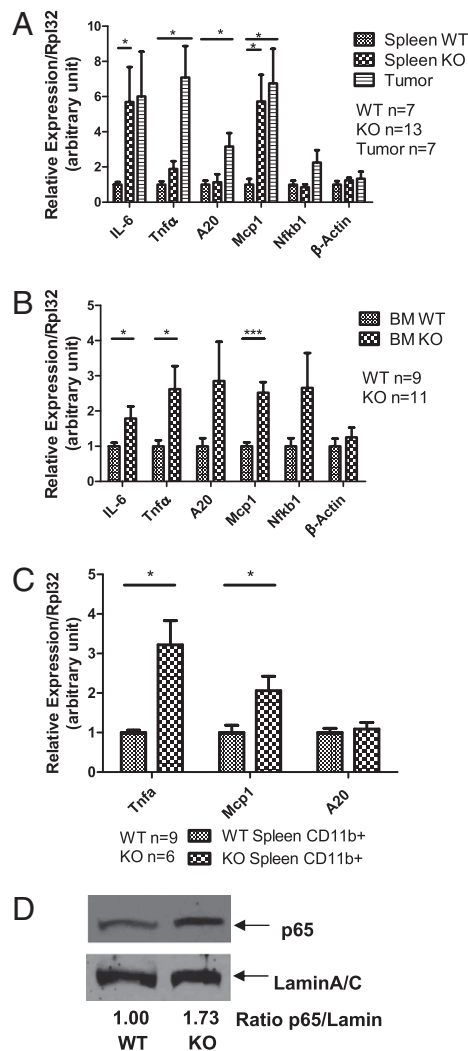
Fig. 4. Spleen and bone marrow cells from miR-146a–deficient mice (KO) show increased activation of the NF-κB–mediated transcription. Mice were 18- to 22-mo-old miR-146a$^{-/-}$ mice (KO) and sex- and age-matched wild-type control mice (WT). Data are shown as mean ± SEM. *n* represents the number of mice analyzed from at least two independent experiments. Student *t* test, *$P < 0.05$, ***$P < 0.005$. (*A*) Gene-expression analysis of NF-κB–responsive genes in wild-type (*n* = 7) nucleated splenocytes, KO (*n* = 13) nucleated splenocytes, and myeloid tumor cells (Tumor, *n* = 7) isolated from KO spleen by gross dissection. (*B*) Gene-expression analysis of NF-κB–responsive genes in wild-type (*n* = 9) and KO (*n* = 11) bone marrow cells. (*C*) Gene-expression analysis of NF-κB–responsive genes in CD11b$^+$ population purified with MACS beads (WT *n* = 9 and KO *n* = 6). (*D*) Western blot analysis of the nuclear protein extracts from wild-type or KO spleen. Data are representative of three independent experiments.

expression of both TRAF6 and IRAK1 at the protein level in bone marrow-derived macrophages from young miR-146a KO mice. However, there was no difference in the serum levels of TNF-α and IL-6 inflammatory cytokine between young wild-type and KO mice without LPS challenge (12). In addition, constitutive NF-κB activity detected by conventional biochemical methods was only consistently noted in spleens with overt myeloid sarcoma (Fig. S4). Based on this evidence, we suggest that the activation of the NF-κB may only become constitutive and significant when KO spleens transition from the premalignant myeloproliferative state to malignant myeloid tumor. Given the long latency and the partial penetrance of the tumor phenotype, there are likely secondary mutations cooperating in the oncogenesis, either complementing the NF-κB activity or amplifying

it, resulting in malignant tumors. It will be interesting to identify secondary mutations driving this progression and malignant transformation.

NF-κB family transcription factors are homo- or heterodimers of five subunits, RelA (p65), Nfkb1 (p50), Nfkb2 (p52), RelB, and c-Rel. Among these subunits, p65 and p50 are thought to play an important role in the induction of many of the inflammatory genes (18). In addition, nfkb1$^{\Delta CT/\Delta CT}$ mice, with elevated p50 activity as a result of targeted deletion of the C-terminal ankyrin repeats, display phenotypes similar to those of miR-146a$^{-/-}$ mice, namely chronic inflammation with splenomegaly and enlarged lymph nodes (19). Moreover, deletion of p50 is able to partially rescue IkBα-deficienct mice, which display constitutive NF-κB activation, increased granulopoiesis, and neonatal lethality (20). Given the importance of the p50 subunit to NF-κB–driven inflammation, we bred miR-146a$^{-/-}$ mice with p50$^{-/-}$ mice to investigate the role of NF-κB activation in the pathogenesis of myeloproliferation in miR-146a-deficient mice. We showed that p50-deficiency effectively rescued myeloproliferation in miR-146a–deficient mice. The rescue seen in miRKO p50HET mice was not consistent and complete, but merely a delay of symptoms, because by about 1 y old, mice in the miRKO p50HET group started to show increased myeloid cells but the DKO mice continued to show consistent rescue of the myeloproliferative phenotype. The 50% increase in spleen weight and the marginal increase in CD11b$^+$ and Ter119$^+$ cells in the spleen of DKO mice, compared with wild-type (Fig. 5 *B* and *C*), suggest that the other pathways and factors other than p50 may also be involved. In addition, p50 deficiency may not rescue all of the phenotypes in miR-146a KO mice, such as autoimmunity as a result of defective regulatory T cells and activated effector T cells, which has been shown to be caused by a different pathway, the STAT1/IFN pathway (21). Autoimmune inflammation may contribute to the modestly increased spleen weight in the DKO mice.

Constitutive NF-κB activation is a well-recognized phenomenon in lymphoid and plasma cell malignancies, but the status of NF-κB activation in myeloid malignancies is less well characterized. Some recent studies have demonstrated constitutive NF-κB activity in cells from high-risk myelodisplastic syndrome, some acute myeloid leukemia cases, and chronic myelogenous leukemia with blast crisis, suggesting that constitutive NF-κB activation may be associated with more advanced myeloid malignancies (6, 22, 23). In many of these cases, the mechanisms for constitutive NF-κB activation remain to be established. It is likely that some of these myeloid malignancies with intrinsic NF-κB activity may have down-regulated miR-146a expression. Indeed, reduced miR-146a has been found in myelodisplastic syndrome with chromosome 5q deletion and a subset of acute myeloid leukemia cases (24, 25).

Based on this work and the work of others, it seems apparent that miR-146a is an important component of immune-cell gene regulation and that its main function is to negatively regulate NF-κB. We demonstrate pathologic states as a consequence of miR-146a deficiency, corroborating work from other groups showing deregulation of this miRNA in human diseases. Further work is required to better understand the pathogenesis of miR-146a–deficient diseases in humans and to develop methods to deliver miR-146a to immune cells to reduce NF-κB activation.

Materials and Methods

Mice. For a description of the miR-146a$^{-/-}$ generation and genotyping, see *SI Materials and Methods* and ref. 12. All experiments with miR-146a$^{-/-}$ and p50$^{-/-}$ (15) mice were approved by the Institutional Animal Care and Use Committee of the California Institute of Technology.

Survival and Tumor Incidence Study. Survival and tumor incidence studies were done by following a cohort of about 40 miR-146a$^{-/-}$ and 40 littermate wild-type control mice for up to 24 mo. Mice were carefully monitored for the development of diseases and were killed when visibly ill. Tumor di-
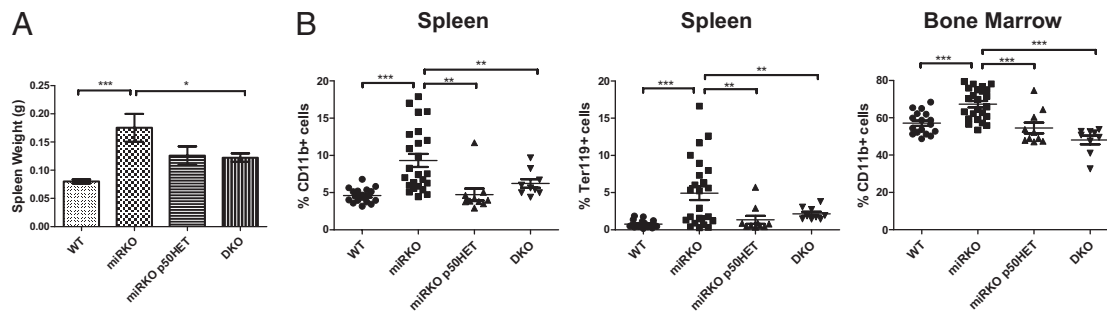
Fig. 5. Reduction in the NF-κB level by deleting the p50 subunit of NF-κB effectively rescues the myeloproliferative phenotype in miR-146a–deficient mice. All mice were 6- to 7-mo-old miR-146a$^{+/+}$, p50$^{+/+}$ (WT), miR-146a$^{-/-}$, p50$^{+/+}$ (miRKO), miR-146a$^{-/-}$, p50$^{+/-}$ (miRKO p50HET), or miR-146a$^{-/-}$, p50$^{-/-}$ (DKO) mice (n = 17 for WT, n = 24 miRKO, n = 10 for miRKO p50HET, and n = 9 for DKO). Data are shown as mean ± SEM from at least three independent experiments. Student t test, *P < 0.05, **P < 0.01, and ***P < 0.005. (*A*) Spleen weight of wild-type, miRKO, miRKO p50HET, and DKO mice. (*B*) Percentage of T cells (defined as CD3ε$^+$), B cells (defined as CD19$^+$), myeloid cells (defined as CD11b$^+$), and erythroid cells (defined as Ter119$^+$) in nucleated spleen and bone marrow cells from wild-type, miRKO, miRKO p50HET, and DKO mice by flow cytometric analysis.

agnosis was based on a combination of gross examination, histological analysis, immunohistochemistry, and flow cytometric analysis.

Tumor Transplantation Experiments. Tumor was grossly dissected from miR-146a$^{-/-}$ mice. Splenic tumor cells (1 × 10^6) or an equal number of wild-type splenocytes were injected into 8- to 12-wk-old Rag2$^{-/-}$γC$^{-/-}$ recipients via retro-orbital vein. For experiments with retro-viral transduction, MIG-Luc (MSCV-IRES-GFP vector expressing firefly luciferase) retroviruses were prepared and used to infect murine cells as previously described (26). Flow cytometry was used to quantify the percentage of infected cells (GFP$^+$) before injection and bioluminescence imaging (Xenogen) was used to monitor

in vivo cell growth in Rag2$^{-/-}$γC$^{-/-}$ recipients weekly for up to 2 mo. Bio-luminescence intensity was quantified with Living Image 2.50.1 (Xenogen). Expanded methods are found in *SI Materials and Methods*.

1. Bartel DP (2009) MicroRNAs: Target recognition and regulatory functions. *Cell* 136: 215–233.
2. O'Connell RM, Rao DS, Chaudhuri AA, Baltimore D (2010) Physiological and pathological roles for microRNAs in the immune system. *Nat Rev Immunol* 10: 111–122.
3. Xiao C, Rajewsky K (2009) MicroRNA control in the immune system: Basic principles. *Cell* 136:26–36.
4. Calin GA, Croce CM (2006) MicroRNA signatures in human cancers. *Nat Rev Cancer* 6: 857–866.
5. Grivennikov SI, Greten FR, Karin M (2010) Immunity, inflammation, and cancer. *Cell* 140:883–899.
6. Braun T, et al. (2006) Targeting NF-kappaB in hematologic malignancies. *Cell Death Differ* 13:748–758.
7. Shen HM, Tergaonkar V (2009) NFkappaB signaling in carcinogenesis and as a potential molecular target for cancer therapy. *Apoptosis* 14:348–363.
8. Liew FY, Xu D, Brint EK, O'Neill LA (2005) Negative regulation of Toll-like receptor-mediated immune responses. *Nat Rev Immunol* 5:446–458.
9. Taganov KD, Boldin MP, Chang KJ, Baltimore D (2006) NF-kappaB-dependent induction of microRNA miR-146, an inhibitor targeted to signaling proteins of innate immune responses. *Proc Natl Acad Sci USA* 103:12481–12486.
10. Williams AE, Perry MM, Moschos SA, Larner-Svensson HM, Lindsay MA (2008) Role of miRNA-146a in the regulation of the innate immune response and cancer. *Biochem Soc Trans* 36:1211–1215.
11. Hou J, et al. (2009) MicroRNA-146a feedback inhibits RIG-I-dependent Type I IFN production in macrophages by targeting TRAF6, IRAK1, and IRAK2. *J Immunol* 183: 2150–2158.
12. Boldin MP, et al. (2011) miR-146a is a significant brake on autoimmunity, myeloproliferation and cancer in mice. *J Exp Med*, in press.
13. Kogan SC, et al.; (2002) Hematopathology subcommittee of the Mouse Models of Human Cancers Consortium Bethesda proposals for classification of nonlymphoid hematopoietic neoplasms in mice. *Blood* 100:238–245.
14. Gerondakis S, et al. (2006) Unravelling the complexities of the NF-kappaB signalling pathway using mouse knockout and transgenic models. *Oncogene* 25:6781–6799.
15. Sha WC, Liou HC, Tuomanen EI, Baltimore D (1995) Targeted disruption of the p50 subunit of NF-kappa B leads to multifocal defects in immune responses. *Cell* 80: 321–330.
16. Cao Z, Xiong J, Takeuchi M, Kurama T, Goeddel DV (1996) TRAF6 is a signal transducer for interleukin-1. *Nature* 383:443–446.
17. Hartupee J, Li X, Hamilton T (2008) Interleukin 1alpha-induced NFkappaB activation and chemokine mRNA stabilization diverge at IRAK1. *J Biol Chem* 283:15689–15693.
18. Hoffmann A, Leung TH, Baltimore D (2003) Genetic analysis of NF-kappaB/Rel transcription factors defines functional specificities. *EMBO J* 22:5530–5539.
19. Ishikawa H, et al. (1998) Chronic inflammation and susceptibility to bacterial infections in mice lacking the polypeptide (p)105 precursor (NF-kappaB1) but expressing p50. *J Exp Med* 187:985–996.
20. Beg AA, Sha WC, Bronson RT, Baltimore D (1995) Constitutive NF-kappa B activation, enhanced granulopoiesis, and neonatal lethality in I kappa B alpha-deficient mice. *Genes Dev* 9:2736–2746.
21. Lu LF, et al. (2010) Function of miR-146a in controlling Treg cell-mediated regulation of Th1 responses. *Cell* 142:914–929.
22. Cilloni D, Martinelli G, Messa F, Baccarani M, Saglio G (2007) Nuclear factor kB as a target for new drug development in myeloid malignancies. *Haematologica* 92: 1224–1229.
23. Braun T, et al. (2006) NF-kappaB constitutes a potential therapeutic target in high-risk myelodysplastic syndrome. *Blood* 107:1156–1165.
24. Garzon R, et al. (2008) MicroRNA signatures associated with cytogenetics and prognosis in acute myeloid leukemia. *Blood* 111:3183–3189.
25. Starczynowski DT, et al. (2010) Identification of miR-145 and miR-146a as mediators of the 5q- syndrome phenotype. *Nat Med* 16:49–58.
26. Rao DS, et al. (2010) MicroRNA-34a perturbs B lymphocyte development by repressing the forkhead box transcription factor Foxp1. *Immunity* 33:48–59.

IMMUNOLOGY